Optimal Time-Varying Heat Transfer in Multilayered Packages With Arbitrary Heat Generations and Contact Resistance

M. Fakoor-Pakdaman[1]
Laboratory for Alternative Energy Conversion (LAEC),
Mechatronic Systems Engineering,
Simon Fraser University,
Surrey, BC V3T 0A3, Canada
e-mail: mfakoorp@sfu.ca

Mehran Ahmadi
Laboratory for Alternative Energy Conversion (LAEC),
Mechatronic Systems Engineering,
Simon Fraser University,
Surrey, BC V3T 0A3, Canada
e-mail: mahmadi@sfu.ca

Farshid Bagheri
Laboratory for Alternative Energy Conversion (LAEC),
Mechatronic Systems Engineering,
Simon Fraser University,
Surrey, BC V3T 0A3, Canada
e-mail: fbagheri@sfu.ca

Majid Bahrami
Laboratory for Alternative Energy Conversion (LAEC),
Mechatronic Systems Engineering,
Simon Fraser University,
Surrey, BC V3T 0A3, Canada
e-mail: mbahrami@sfu.ca

Integrating the cooling systems of power electronics and electric machines (PEEMs) with other existing vehicle thermal management systems is an innovative technology for the next-generation hybrid electric vehicles (HEVs). As such, the reliability of PEEM must be assured under different dynamic duty cycles. Accumulation of excessive heat within the multilayered packages of PEEMs, due to the thermal contact resistance between the layers and variable temperature of the coolant, is the main challenge that needs to be addressed over a transient thermal duty cycle. Accordingly, a new analytical model is developed to predict transient heat diffusion inside multilayered composite packages. It is assumed that the composite exchanges heat via convection and radiation mechanisms with the surrounding fluid whose temperature varies arbitrarily over time (thermal duty cycle). As such, a time-dependent conjugate convection and radiation heat transfer is considered for the outer-surface. Moreover, arbitrary heat generation inside the layers and thermal contact resistances between the layers are taken into account. New closed-form relationships are developed to calculate the temperature distribution inside multilayered media. The present model is used to find an optimum value for the angular frequency of the surrounding fluid temperature to maximize the interfacial heat flux of composite media; up to 10% higher interfacial heat dissipation rate compared to constant fluid-temperature case. An independent numerical simulation is also performed using Comsol Multiphysics; the maximum relative difference between the obtained numerical data and the analytical model is less than 6%. [DOI: 10.1115/1.4028243]

Keywords: multilayered composite systems, transient conduction, thermal contact resistance, electronic packages, dynamic thermal response, integrated thermal management

1 Introduction

Integration of component thermal management technologies for new propulsion systems is a key to developing innovative technology for the next-generation HEVs, electric vehicles (EVs), and fuel cell vehicles (FCVs). Current hybrid systems use a separate low-temperature liquid cooling loop for the PEEM [1,2]. However, utilizing an integrated cooling loop for an HEV addresses the cost, weight, size, and fuel consumption [2–4]. As such, the cooling systems of PEEM can be integrated with (i) the air conditioning system via a low-temperature coolant loop and (ii) the internal combustion engine (ICE) via a high-temperature cooling system. Typically, steady-state scenarios were considered for the thermal management of conventional vehicles [3,5]. However, within the context of "integrated thermal management," the evaluation over a transient thermal duty cycle is important. This is attributed to the fact that certain components may not experience peak thermal loads over steady-state cases or at the same time during a vehicle driving cycle [2]. Misalignment of the peak heat loads leads to variable time-dependent coolant temperature for PEEM over a transient duty cycle. For instance, for the above-mentioned high-temperature cooling loop of PEEM and ICE, the coolant temperature of the electric machine was reported to fluctuate between 80°C and 110°C, depending upon the functionality of ICE during the studied duty cycle [3].

To successfully integrate dynamic PEEM cooling systems concept into vehicle applications, the thermal limitations of the semiconductor devices must be addressed [6]. For critical semiconductor devices such as insulated gate bipolar transistors (IGBTs) in an HEV, McGlen et al. [7] predicted heat fluxes of $150 - 200(\mathrm{W/cm^2})$ and pulsed transient heat loads with heat fluxes up to $400(\mathrm{W/cm^2})$. According to Samsung technologists, the next-generation semiconductor technology costs about $10 billion to create [6]. Alternatively, utilization of multilayered packages is recognized as an innovative technique for the thermal management of semiconductor devices, which also results in improved performance through lowering of signal delays and increasing processing speed. However, due to the dynamic unsteady characteristics of the power electronics inside HEVs/EVs/FCVs, accumulation of excessive heat within the multilayered packages as a result of thermal contact resistance between the layers as well as variable temperature of the coolant is the main challenge that needs to be addressed [6–12]. One important aspect of the thermal design of such dynamic multilayered systems is the ability to obtain an accurate transient temperature solution of the packages beforehand in order to sustain the reliability of the packages albeit for a more simplified configuration.

Transient heat conduction in multilayered packages has been the subject of numerous studies, e.g., Refs. [13–28]. De Monte

[1]Corresponding author.

Contributed by the Heat Transfer Division of ASME for publication in the Journal of Heat Transfer. Manuscript received November 5, 2013; final manuscript received July 25, 2014; published online April 21, 2015. Assoc. Editor: Jim A. Liburdy.

[13] presented a summary of different analytical approaches that can be adopted to analyze transient heat conduction. Laplace transform method [14], Green's function approach [15], and finite integral transform technique [16] are useful in single layer problems. However, they cannot be readily adopted to analyze multilayered heat conduction problems [13]. In fact, quasi-orthogonal expansion technique and separation-of-variables methods are the most elegant and straightforward approaches to analyze multiregion problems [17–23]. However, such approaches can only address homogeneous or constant boundary conditions, see Refs. [24–28]. Although encountered quite often in practice, nonlinear and time-dependent boundary conditions always posed challenge to the analysis of transient heat conduction in multilayered composites. The pertinent literature has been limited to constant/simplified boundary conditions, i.e., isothermal, isoflux, or convective cooling surfaces. The solution to time-dependent heat flux or boundary temperature cases can be found by Duhamel's theorem [14]. However, time-dependent convective cooling case, which inevitably occurs during a transient duty cycle for multilayered packages of PEEM, cannot be treated by such approach [29]; this adds extra complexity to the problem. To the best knowledge of the authors, there are only few works on transient heat conduction in multilayered composites with heat generation subjected to nonlinear or time-dependent convective–radiative cooling. Our literature review indicates that

- there is no analytical model to predict the thermal behavior of composite media with heat generation subjected to time-dependent conjugate convection–radiation.
- effects of radiation on thermal characteristics of a multilayered composite over a transient thermal duty cycle have not been considered in the existing models.
- effects of thermal contact resistance, at the interfaces between layers, have not been considered in modeling of multilayered composites under dynamic thermal load, or time-dependent boundary conditions.

To develop the present analytical model, a general time-dependent temperature is assumed for the surrounding fluid which is decomposed into simple oscillatory functions using a cosine Fourier transformation [30]. As such, conjugate radiation–convection heat transfer boundary condition is considered for the outer boundary of a composite medium. The quadratic behavior of radiation is linearized to address the boundary value problem. A quasi-orthogonal expansion technique [18] is used to find the eigenvalues of the closed-form analytical solution. Complex exponential form of the boundary condition is taken into account along with a periodic temperature response inside the media. Separation of variables method is employed and following [20] the associated discontinuous-weighting functions are found to make the obtained eigenfunctions orthogonal. Closed-form relationships are obtained for temperature distribution inside the multilayered region with arbitrary heat generations and contact resistances under time-dependent conjugate radiation–convection.

2 Governing Equations

Shown in Fig. 1 is a multilayered composite region involving M parallel layers of slabs, concentric cylinders, or spheres with thermal contact resistance at the interfaces. In addition, without loss of generality, it is assumed that the surface x_0 represents the coordinate origin, $x_0 = 0$. In case of composite slabs, $x = x_0$ is thermally insulated, while it is the symmetry line in case of concentric cylinders, and center in case of spheres. Moreover, the layer interfaces in the x-direction are $x_1, x_2, ..., x_j$, where $j = 1, 2, ..., M$. Let k_j and α_j be the thermal conductivity and the thermal diffusivity of the jth layer, respectively. Initially, the multilayered composite, which is confined to the domain $x_0 \le x \le x_M$, is at a uniform temperature T_0. It is assumed that both convection and radiation heat transfer occurs between the outer-surface boundary, $x = x_M$, that is wetted by the surrounding fluid. An arbitrary time-dependent temperature is considered for the surrounding fluid as given below:

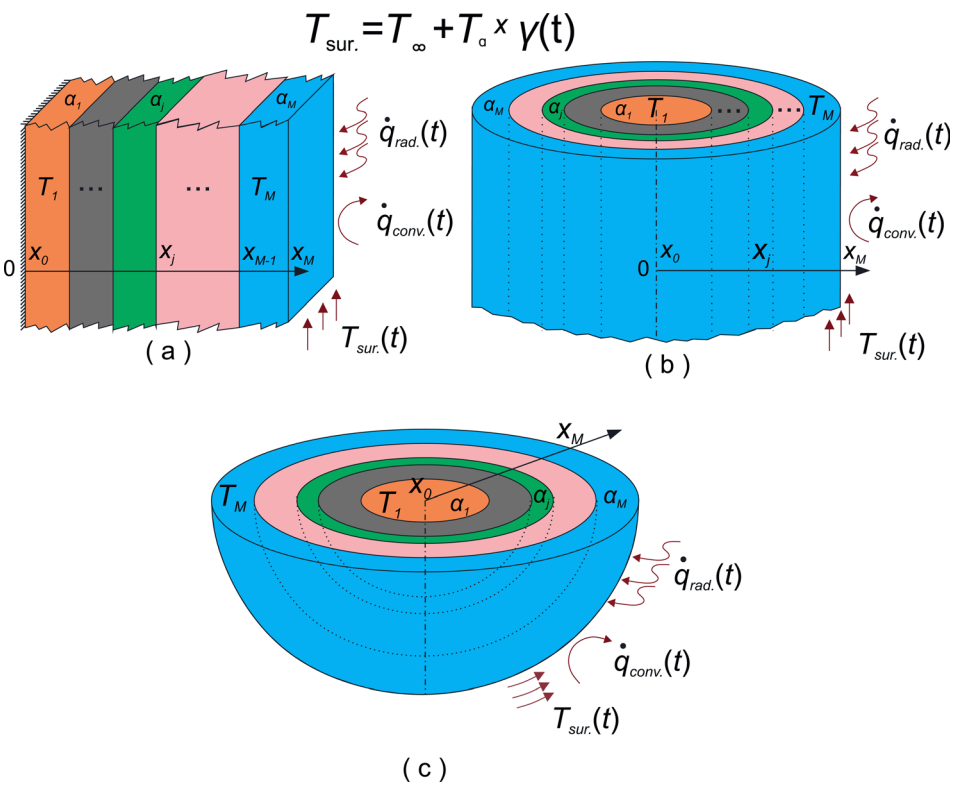

Fig. 1 Schematic of multilayered composites in (*a*) Cartesian, (*b*) cylindrical, and (*c*) spherical coordinate systems

$$T_{\text{sur.}} = T_\infty + T_a \times \gamma(t) \tag{1}$$

where $T_{\text{sur.}}$ is the time-varying surrounding temperature, $T_\infty[K]$ is a constant, $T_a[K]$ is the amplitude of the variation of the surrounding fluid temperature, and $\gamma(t)$ is an arbitrary function of time, respectively. Other assumptions used in the proposed unsteady heat conduction model are

- constant thermo-physical properties for all M layers.
- the thickness of the multilayered composite is sufficiently thin in x-direction compared to the other directions, i.e., one-dimensional heat transfer.

As such, the mathematical formulation of the transient heat conduction problem herein under discussion becomes

$$\frac{1}{\alpha_j}\frac{\partial T_j(x,t)}{\partial t} = \nabla^2 T_j(x,t) + \frac{\dot{q}_j(x)}{k_j} \quad x_{j-1} \le x \le x_j, t > 0 \quad j = 1, 2, ..., M \tag{2}$$

The boundary conditions are

$$\frac{\partial T_1(0,t)}{\partial x} = 0 \quad \text{at} \quad x = 0, t > 0 \tag{2a}$$

$$-k_j\frac{\partial T_j}{\partial x} = \delta_j \times \left[T_j(x_j,t) - T_{j+1}(x_j,t)\right] \quad j = 1,2,3,...,(M-1) \quad \text{and} \quad t > 0 \tag{2b}$$

$$k_j\frac{\partial T_j(x_j,t)}{\partial x} = k_{j+1}\frac{\partial T_{j+1}(x_j,t)}{\partial x} \quad j = 1,2,3,...,(M-1) \quad \text{and} \quad t > 0 \tag{2c}$$

$$\underbrace{-k_M\frac{\partial T_M}{\partial x}\Big|_{(x_m,t)}}_{\dot{q}_{\text{cond.}}} = \underbrace{h_c\left[T_M(x_m,t) - T_{\text{sur.}}(t)\right]}_{\dot{q}_{\text{conv.}}} + \underbrace{\sigma\varepsilon\left[T_M^4(x_m,t) - T_{\text{sur.}}^4(t)\right]}_{\dot{q}_{\text{rad.}}} \quad \text{at} \quad x = x_M, t > 0 \tag{2d}$$

The initial condition is

$$T_j(x,0) = T_0 \quad x_{j-1} \le x \le x_j, \quad j = 1,2,...,M, \quad \text{and} \quad t = 0 \tag{2e}$$

where

$$\nabla^2 \equiv \frac{1}{x^p}\frac{\partial}{\partial x}\left(x^p\frac{\partial}{\partial x}\right) \tag{3}$$

is the one-dimensional Laplace differential operator, $T_j(x,t)$ is the instantaneous temperature of the jth layer at depth x and time t, and x_{j-1}, x_j denote the coordinates of the jth layer surfaces. In addition, $\delta_j(\text{W/m}^2\text{K})$ is the contact conductance between the jth and $j+1$th layers, ε is the emissivity of the Mth layer (outer surface), $\sigma(\text{W/m}^2\text{K}^4)$ denotes the Stephan–Boltzmann constant, and $h_c(\text{W/m}^2\text{K})$ refers to the convective heat transfer coefficient between the Mth layer and the surrounding fluid. The following dimensionless variables are defined:

$$Fo = \frac{\alpha_1 t}{x_1^2}, \quad \eta = \frac{x}{x_1}, \quad \mu_j = \frac{\alpha_j}{\alpha_1}, \quad K_j = \frac{k_{j+1}}{k_j}, \quad \text{Bi}_r = \frac{h_r x_1}{k_M}, \quad \text{Bi}_c = \frac{h_c x_1}{k_M} \quad \Lambda_j = \frac{\delta_j x_1}{k_j}, \quad \theta = \frac{T - T_0}{T_\infty - T_0}, \quad \omega = \Omega\frac{x_1^2}{\alpha_1},$$
$$g_j(\eta) = \mu_j\frac{\dot{q}(x)x_1^2}{k_j(T_\infty - T_0)}, \quad \Delta T_R = \frac{\text{Bi} \times T_a}{T_\infty - T_0}$$

For a constant surrounding fluid temperature, Chapman [31] showed that when the initial temperature of the medium is close to the surrounding fluid temperature, i.e., $T_0/T_{\text{sur}} > 0.75$, the forth-order effect of radiation heat transfer can be linearized, as an approximation. The validity of this assumption has been tested in numerous works, e.g., see Refs. [19–21]. In this paper, we consider the cases in which the ratio of initial temperature and maximum surrounding temperature is higher than 0.75, i.e., $T_0/T_{\text{sur,max}} > 0.75$; this justifies linearization of the radiation effects [31–33]. Therefore, Eq. (2*d*), time-dependent conjugate convective–radiative boundary condition, can be linearized as Eq. (4).

$$-k_M\frac{\partial T_M}{\partial x}\Big|_{(x_m,t)} = (h_c + h_r) \times \left[T_M(x_m,t) - T_{\text{sur.}}(t)\right] \quad \text{at} \quad x = x_M, t > 0 \tag{4}$$

where $h_r[\text{W/m}^2\text{K}]$ is the transformed radiation heat transfer coefficient defined as follows [28]:

$$h_r = 4\varepsilon\sigma T_{\text{sur.,max}}^3 \tag{5}$$

where $T_{\text{sur.,max}}$ is the maximum surrounding fluid temperature during a transient duty cycle. It is evident that when radiation is neglected, $h_r \approx 0$, Eq. (4) reduces to time-dependent pure-convection boundary condition. Nonetheless, the dimensionless form of the energy equation, Eq. (2), becomes

$$\frac{\partial\theta_j}{\partial Fo} = \mu_j\frac{1}{\eta^p}\frac{\partial}{\partial\eta}\left(\eta^p\frac{\partial\theta_j}{\partial\eta}\right) + g_j(\eta) \quad 0 \le \eta \le \frac{x_M}{x_1}, \quad Fo > 0 \quad j = 1,2,...,M \tag{6}$$

where θ_j is the dimensionless temperature of the jth layer, Fo is the dimensionless time, η is the dimensionless coordinate, and $g_j(\eta)$ is the dimensionless heat generation inside the jth layer. Equation (6) is subjected to the following dimensionless initial and boundary conditions:

$$\theta_j(\eta,0) = 0 \quad \frac{x_{j-1}}{x_1} \le \eta \le \frac{x_j}{x_1}, \quad j = 1,2,3,...,M \quad \text{and} \quad Fo = 0 \tag{6a}$$

$$\frac{\partial\theta_1}{\partial\eta} = 0 \quad \text{at} \quad \eta = 0, \quad Fo > 0 \tag{6b}$$

$$\frac{\partial\theta_j}{\partial\eta} = \Lambda_j\left[\theta_{j+1}(\eta = x_j/x_1, Fo) - \theta_j(\eta = x_j/x_1, Fo)\right] \quad j = 1,2,3,...,(M-1), \quad \text{and} \quad Fo > 0 \tag{6c}$$

$$\frac{\partial\theta_j(\eta = x_j/x_1, Fo)}{\partial\eta} = K_j\frac{\partial\theta_{j+1}(\eta = x_j/x_1, Fo)}{\partial\eta} \quad j = 1,2,3,...,(M-1), \quad \text{and} \quad Fo > 0 \tag{6d}$$

$$\frac{\partial\theta_M(\eta = x_M/x_1, Fo)}{\partial\eta} + \text{Bi} \times \theta_M(\eta = x_M/x_1, Fo) = \text{Bi} + \Delta T_R \times \gamma(Fo) \quad \text{at} \quad \eta = \frac{x_M}{x_1}, \quad Fo > 0 \tag{6e}$$

where $\Lambda_j = \delta_j x_1/k_j$ is the dimensionless contact conductance between the jth and $j+1$th layers, $\text{Bi} = (h_r + h_c)x_1/k_M$ is the combined radiative–convective Biot number, and $\Delta T_R = \text{Bi} \times T_a/T_\infty - T_0$ is a dimensionless number. For sake of generality, the imposed boundary condition, Eq. (6*e*), is considered as follows:

$$A_{\text{out}} \times \frac{\partial\theta_M(\eta = x_M/x_1, Fo)}{\partial\eta} + B_{\text{out}} \times \theta_M(\eta = x_M/x_1, Fo) = C_{\text{out}} + \Delta T_R \times \gamma(Fo) \quad \text{at} \quad \eta = \frac{x_M}{x_1}, \quad Fo > 0, \quad B_{\text{out}} \neq 0 \tag{7}$$

where A_{out}, B_{out}, and C_{out} are constant values. It should be noted that when $A_{out} = 1$ and $B_{out} = C_{out} = Bi$, Eq. (7) reduces to Eq. (6*e*). In addition, when $A_{out} = 0$, the boundary condition, Eq. (7), indicates the case in which the outer-surface boundary of a composite medium, $x = x_M$, undergoes dynamic time-dependent temperature.

3 Model development

A new model is developed to predict the thermal response of a multilayered composite in Cartesian, cylindrical, and spherical coordinates. It is assumed that the multilayered composite transfers heat via convection and radiation to the surrounding fluid whose temperature varies arbitrarily over time. Thermal contact resistances between the layers and arbitrary heat generation inside each layer are taken into consideration. The methodology is presented for: (i) a composite medium with arbitrary number of layers, The Appendix; and (ii) a composite slab (a two-die stack) consisting of two parallel layers with arbitrary heat generations and a thermal interface material (TIM) as an example in Sec. 3.1, see Fig. 2. It should be noted that the TIM layer is used to schematically represent the thermal contact resistance at the interface.

3.1 A Two-Layered Composite Slab. In this section, arbitrary heat generations inside each layer $g_j(\eta)$ and contact conductance between the layers, Λ_1, are taken into account. A harmonic temperature is considered for the surrounding fluid, Eq. (A1). Based on Eq. (A6), the following transcendental equation is obtained to evaluate the eigenvalues:

$$\frac{\tan\left(\frac{\lambda_n}{\sqrt{\mu_2}}\right) - \frac{\sqrt{\mu_2}}{K}\tan(\lambda_n) - \frac{\lambda_n}{\Lambda_1}\tan(\lambda_n)\tan\left(\frac{\lambda_n}{\sqrt{\mu_2}}\right)}{1 + \frac{\sqrt{\mu_2}}{K}\tan(\lambda_n)\tan\left(\frac{\lambda_n}{\sqrt{\mu_2}}\right) - \frac{\lambda_n}{\Lambda_1}\tan(\lambda_n)} = \frac{\left(\frac{A_{out}\lambda_n}{\sqrt{\mu_2}}\right)\tan\left(\frac{\lambda_n}{\sqrt{\mu_2}}\eta_2\right) - B_{out}}{\left(\frac{A_{out}\lambda_n}{\sqrt{\mu_2}}\right) + B_{out}\tan\left(\frac{\lambda_n}{\sqrt{\mu_2}}\eta_2\right)} \tag{8}$$

Thus, with respect to Eq. (A18), the temperature distribution inside the entire medium is obtained as follows:

$$\theta_j(\eta, Fo) = \frac{C_{out}}{B_{out}} \times \cos(\omega Fo + \varphi) + \sum_{n=1}^{\infty} R_{jn}(\eta)\left\{\begin{array}{l} A_n \times \cos(\varphi) \times e^{-(\lambda_n^2 Fo)} - \\ E_n\left\{\frac{\omega \times [\cos(\omega Fo + \varphi)] - \lambda_n^2 \times [\sin(\omega Fo + \varphi)]}{\lambda_n^4 + \omega^2}\right\} + \frac{G_n}{\lambda_n^2}\end{array}\right\} \quad j = 1, 2 \tag{9}$$

The definition of the parameters used in Eq. (9) is provided in Table 1. The constants C_{2n} and D_{2n} are evaluated by applying Eq. (A4)

$$C_{2n} = \cos(\lambda_n)\cos\left(\frac{\lambda_n}{\sqrt{\mu_2}}\right) + \frac{\sqrt{\mu_2}}{\lambda_n}\sin(\lambda_n)\sin\left(\frac{\lambda_n}{\sqrt{\mu_2}}\right) - \frac{\lambda_n}{\Lambda_1}\sin(\lambda_n)\cos\left(\frac{\lambda_n}{\sqrt{\mu_2}}\right) \tag{10a}$$

$$D_{2n} = \cos(\lambda_n)\sin\left(\frac{\lambda_n}{\sqrt{\mu_2}}\right) - \frac{\sqrt{\mu_2}}{\lambda_n}\sin(\lambda_n)\cos\left(\frac{\lambda_n}{\sqrt{\mu_2}}\right) - \frac{\lambda_n}{\Lambda_1}\sin(\lambda_n)\sin\left(\frac{\lambda_n}{\sqrt{\mu_2}}\right) \tag{10b}$$

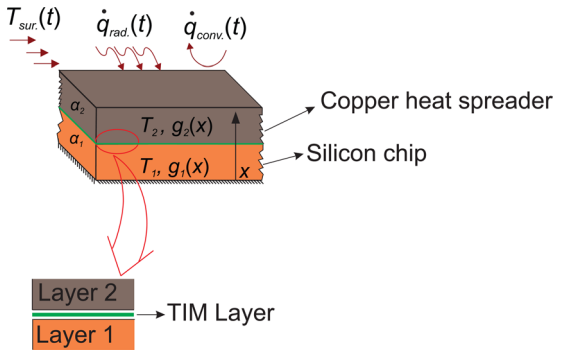

Fig. 2 Schematic of a two-die stack, and TIM subjected to time-dependent conjugate convection–radiation with a surrounding fluid

4 Numerical Study

An independent numerical simulation of the present unsteady one-dimensional heat conduction inside a two-layered slab is also conducted using the commercially available software, Comsol Multiphysics. The thermal contact resistance between the layers is modeled by a thin thermally resistive layer. Besides, the heat generation inside the layers is taken into consideration. Furthermore, the assumptions stated in Sec. 2 are used in the numerical analysis. Harmonic and arbitrary time-dependent temperatures, Eqs. (12) and (13), are considered for the surrounding fluid. Conjugate convective–radiative heat transfer between the outer-surface boundary and the surrounding fluid are taken into account. Grid independency of the results was also verified by using three different grid sizes, namely, 1500, 2000, and 2500 cells. Since there was a little difference between the simulation results from the fine and medium-sized grids (only 1% at the most), the medium grid size was chosen for modeling to reduce the computational time. The geometrical and thermal properties used in the baseline case for numerical simulation of a two die stack are listed in Table 2. Such geometry encountered quite often in a range of practical applications including power electronics cooling, microelectronics, IGBT packages in HEVs, and high power applications, see Refs. [34] and [35]. The values associated with the TIM layer for the base-line case are in accordance with the properties of The Dow corning TC-5022 which is thermal grease extensively used in the aforementioned applications, see Ref. [34]. The convective heat transfer coefficient is also assumed as, $h_c = 18,000(\mathrm{W/m^2/K})$ [36], for the base-line case since this is the average heat transfer coefficient in most electronic cooling applications, see Refs. [35] and [37]. In addition, following Ref. [35], heat flux of $200(\mathrm{W/cm^2})$ is considered for the silicon chip heat generation as a typical peak value that occurs in the IGBTs. The

Table 1 Definition of the parameters in Eq. (9)

Parameter	definition
R_{1n}	$\cos(\lambda_n\eta)$
R_{2n}	$C_{2n}\cos\left(\lambda_n\eta/\sqrt{\mu_2}\right)+D_{2n}\sin\left(\lambda_n\eta/\sqrt{\mu_2}\right)$
E_n	$\omega C_{\text{out}}/B_{\text{out}}\times\int_0^1 R_{1n}(\eta)d\eta+(K_1/\mu_2)\int_1^{\eta_2}R_{2n}(\eta)d\eta/\int_0^1 R_{1n}^2(\eta)d\eta+(K_1/\mu_2)\int_1^{\eta_2}R_{2n}^2(\eta)d\eta$
G_n	$\int_0^1 g_1(\eta)R_{1n}(\eta)d\eta+(K_1/\mu_2)\int_1^{\eta_2}g_2(\eta)R_{2n}(\eta)d\eta/\int_0^1 R_{1n}^2(\eta)d\eta+(K_1/\mu_2)\int_1^{\eta_2}R_{2n}^2(\eta)d\eta$
A_n	$A_n=1/\cos(\varphi)\times\left\{E_n\left[\omega\times\cos(\varphi)-\lambda_n^2\times\sin(\varphi)/\omega^2+\lambda_n^4-\cos(\varphi)/\omega\right]-G_n/\lambda_n^2\right\}$

Table 2 Values of the thermal and geometrical properties for the baseline case in the numerical simulation

Layer, j	Density, $\rho(\text{kg/m}^3)$	Thermal conductivity, $k(\text{W/m/K})$	Thermal capacity, $c_p(\text{J/kg/K})$	Thickness, $x(\text{mm})$	Heat load $[\text{W/cm}^2$
1 (silicon chip), [37]	2330	148	712	0.75	200
TIM Layer (Dow Corning TC-5022), [38]	—	4	—	0.15	—
2 (copper heat spreader), [37]	8933	401	385	1	—

$h_c=18,000\left(\text{W/m}^2/\text{K}\right), T_0=300(\text{K})$

maximum relative difference between the analytical results and the numerical data is less than 6%; more detail is presented in Sec. 5.

5 Results and Discussion

The analytical model described in Sec. 3.1, for two parallel slabs (a two-die stack) are represented here in graphical form and compared with the numerical data obtained in Sec. 4. As such, the results are presented for: (i) a harmonic surrounding fluid temperature, and (ii) arbitrary time-dependent surrounding fluid temperature. In fact, the former case study indicates a harmonic conjugate convective–radiative boundary condition, and the latter accounts for an arbitrary time-dependent conjugate convection–radiation. A code is developed using commercially available software MAPLE 15 to solve the transcendental relationship, Eq. (8). Our study shows that using the first 50 terms in the series solution, Eq. (9), is accurate enough to obtain the temperature distribution inside the media up to four decimal digits. Note that the number of series terms can be notably reduced for large time scales since for large values of n, $\lambda_n\to\infty$, and the exponential term in Eq. (A18) drops remarkably.

5.1 Harmonic Surrounding Fluid Temperature. In this case, the surrounding fluid temperature is considered harmonically as follows:

$$T_{\text{sur.}}(t)=T_\infty+T_a\times\cos(\Omega t+\varphi) \tag{11}$$

The dimensionless form of Eq. (11) is as given below:

$$\theta_{\text{sur.}}=\frac{T_{\text{sur.}}-T_0}{T_\infty-T_0}=1+\Delta T_a\times\cos(\omega Fo+\varphi) \tag{12}$$

where $\omega=\Omega\times x_1^2/\alpha_1$ and $\Delta T_a=T_a/T_\infty-T_0$ are the dimensionless angular frequency and amplitude of the surrounding fluid temperature, respectively. As such, effects of thermal contact resistance on the thermal characteristics of the studied composite medium are shown. In addition, optimum conditions are found to maximize the amplitude of the interfacial heat flux of a composite medium under harmonic boundary condition.

5.1.1 Effects of the Thermal Contact Resistance, $\Lambda_j=\delta_j x_1/k_1$. Figure 3 shows the variations of the dimensionless temperature of the insulated axis $\theta_{\eta=0}$, Eq. (9), against the Fourier number for different values of dimensionless conductance between the layers, $\Lambda_1=\delta_1 x_1/k_1$. Harmonic temperature is assumed for the surrounding fluid temperature, Eq. (12), where $T_\infty=350(\text{K}), T_a=50(\text{K})$, and $\Omega=49.2(\text{rad/s})$. It should be noted that when $\Lambda_1\to\infty$, the thermal contact resistance between the layers becomes negligible, and the present model yields the solution for a two-layer slab with perfect contact at the interface. As shown in Fig. 3, there is a good agreement between the analytical results, and the obtained numerical data; maximum relative difference less than 2.7%. The following values are assumed for the dimensionless variables: $\mu_2=\alpha_2/\alpha_1=1.3$, $K_1=k_2/k_1=2.71$, $\eta_2=x_2/x_1=2.33$, and $\omega=0.1\pi$. To compare the analytical results with the numerical data, according to Ref. [34], the thermal conductivity of the resistive layer is considered as $4, 2, 0.5[\text{W/m}\cdot\text{K}]$, which correspond to $\Lambda_1=0.135, 0.0676$, and 0.0169, respectively.

As expected, the higher the contact conductance between the layers, the higher the amplitude of the temperature field inside the composite medium would become. The peak-shifting trend of the insulated axis temperature for different values of dimensionless interface conductance shows a "thermal lag" of the system caused by the thermal contact resistance. Irrespective of thermal contact resistance, the temperature inside the media fluctuates with the angular frequency of the surrounding temperature. In addition, as $\Lambda_1\to 0$, the interface acts as a thermal insulation, and the temperature of the silicon chip is significantly less than that of high conductance at the interface.

5.1.2 Optimization of the System. When a multilayered package is exposed to a fluid with harmonic temperature, there is an optimum value for the angular frequency at which the amplitude of the interfacial heat flux is maximized. This optimum angular frequency maximizes the heat flux for given values of the dimensionless parameters K_1, μ_2, and η_2. Figure 4 shows the variations of the maximum interfacial heat flux versus the angular frequency for different values of the thickness ratio. The thermal contact resistance between the layers, and the heat generation inside the layers are neglected. Here the values of the thermal conductivity and diffusivity ratios are $K_1=k_2/k_1=2.71$ and $\mu_2=\alpha_2/\alpha_1=1.3$, respectively, for the two-die stack described earlier.

As the thickness ratio increases, the maximum interfacial heat flux decreases. This is attributed to the thermal inertia of the upper layer which decreases the rate of heat transfer at the interface. For low thickness ratios, i.e., $\eta\le 2$, as the angular frequency increases, the interfacial heat flux starts increasing to form a hump

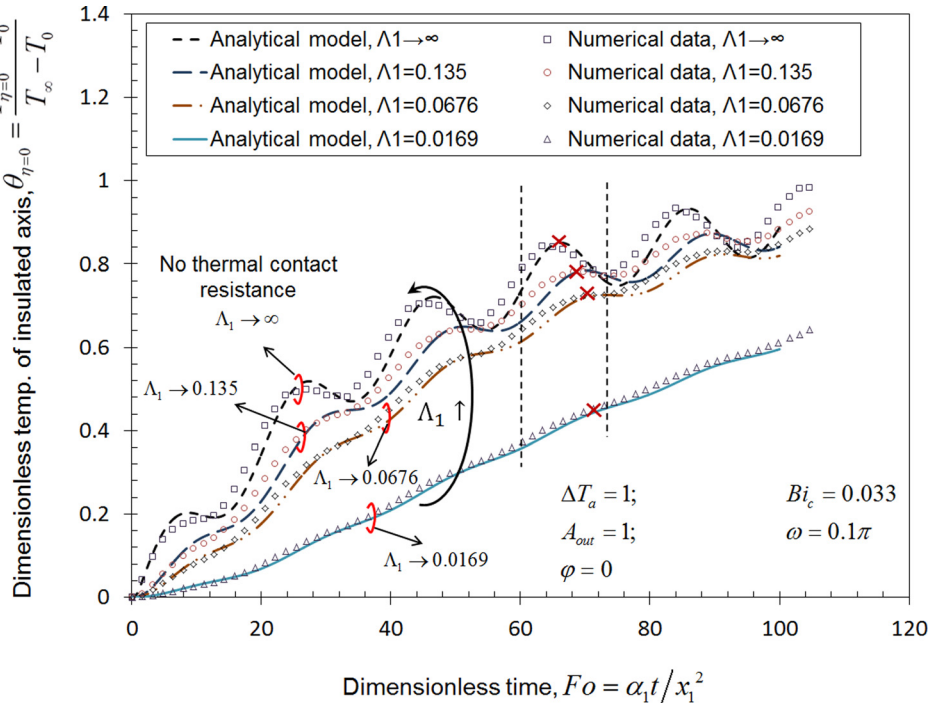

Fig. 3 Variations of the dimensionless temperature of the insulated axis $\theta_{\eta=0}$, Eq. (9), against the Fourier number for different values of the dimensionless conductance between the layers, Λ_1

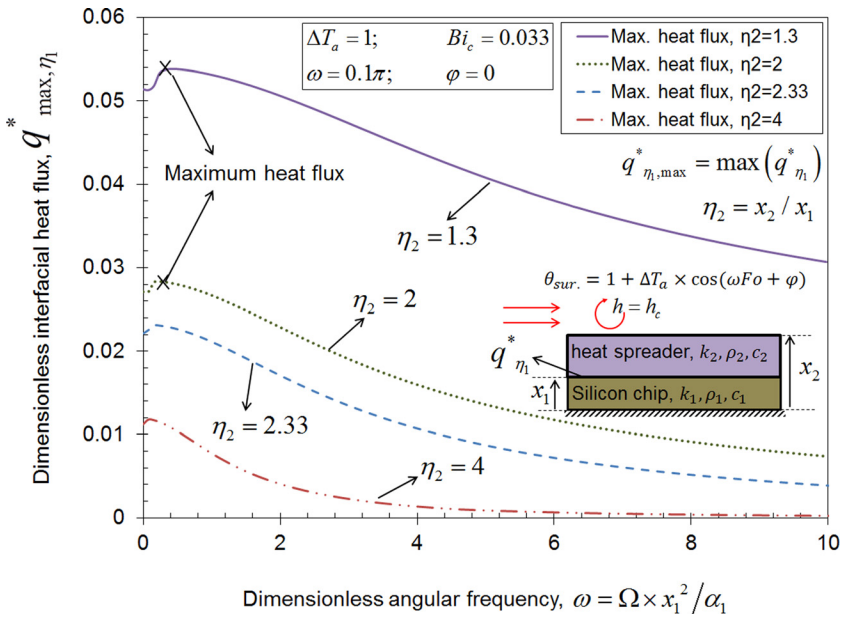

Fig. 4 Variations of the maximum interfacial heat flux, Eq. (A12), versus the angular frequency for different values of the thickness ratios

at the optimum angular frequency, $\omega \approx 0.3$. Beyond the optimum point, the interfacial heat flux decreases until it asymptotically approaches the value associated with the constant term of the surrounding fluid temperature. Moreover, variable coolant temperature over time does not necessarily decrease the performance of multilayered electronic packages during a thermal transient duty cycle. In fact, when the coolant temperature varies with the optimum angular frequency, i.e., $\omega \approx 0.3$, the amplitude of heat dissipation from a multilayered package increases compared to the that of constant surrounding fluid temperature. For high thickness

Table 3 Parameters in Eq. (13)

$T_\infty = 373$(K)	Ω_1(rad/s)	Ω_2(rad/s)	Ω_3(rad/s)	Ω_4(rad/s)
	49.2	246	492	24.6
$T_0 = 300$(K)	$(T_a)_1$(K)	$(T_a)_2$(K)	$(T_a)_3$(K)	$(T_a)_4$(K)
	15	20	5	15
	φ_1(rad)	φ_2(rad)	φ_3(rad)	φ_4(rad)
	0	$-\pi/8$	$-\pi/4$	$-\pi/2$

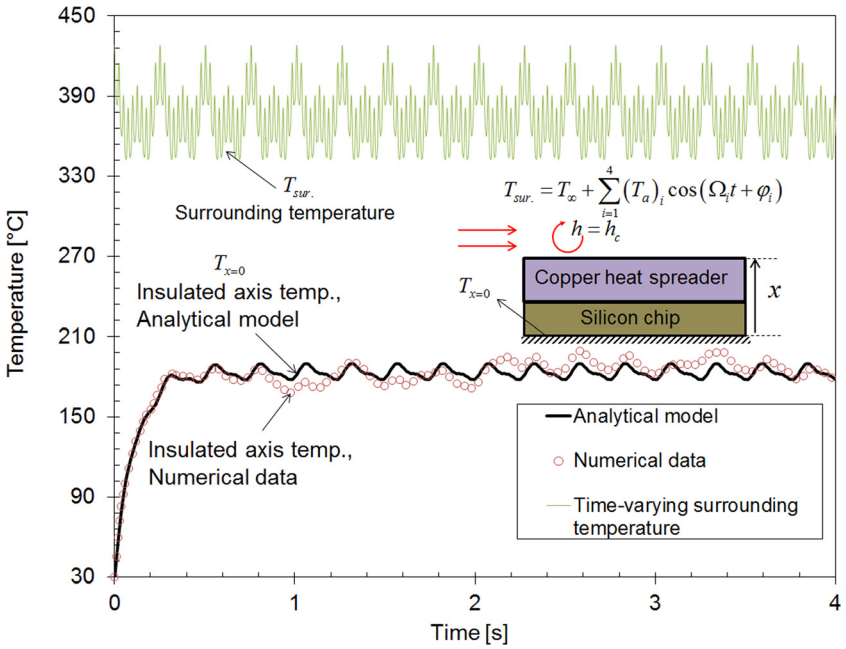

Fig. 5 Variations of the insulated axis temperature T_{x_0}, Eq. (9), versus time for an arbitrary time-dependent conjugate convective–radiative boundary condition, Eq. (15)

ratios, i.e., $\eta > 2$, the maximum heat transfer occurs at $\omega = 0$. This is attributed to the high thermal inertia ratio of the upper to the bottom layer, which reduces the fluctuations caused by the periodic term in the surrounding fluid temperature. Besides, the higher the angular frequency, the lower the interfacial heat flux. This happens due to the fact that the composite medium does not follow the details of the "transient heat transfer" for high angular frequencies. Therefore, the effects of the harmonic excitation decreases, and the interfacial heat flux yields the response for constant surrounding fluid temperature. Furthermore, for given values of thermal conductivity, thermal diffusivity, and thickness ratio, there is an optimum angular frequency which maximizes the interfacial heat flux amplitude. These points are marked in Fig. 4.

5.2 Arbitrary Time-Dependent Surrounding Temperature. The coolant temperature of the multilayered packages associated with the PEEMs of HEVs varies arbitrarily over time. Thus, a superposition technique is applied to the results of the harmonic boundary condition, Sec. 5.1, using the cosine Fourier transformation [30]. It is intended to obtain the temperature distribution inside a two-die stack exchanging heat with a fluid whose temperature varies arbitrarily over time. Following Ref. [34], the surrounding temperature is assumed to fluctuates around 100 [°C]. The analytical results are compared with the numerical simulation data obtained in Sec. 4. The results presented here are dimensional; we believe this will provide a better sense for the problem herein under consideration. The temperature of the surrounding fluid is assumed to vary arbitrarily over time as follows:

$$T_{\text{sur.}} = T_\infty + \sum_{i=1}^{4} (T_{\text{a}})_i \cos(\Omega_i t + \varphi_i) \tag{13}$$

The values of the parameters in Eq. (13) are presented in Table 3. The geometrical and thermophysical properties of the composite medium are previously given in Table 2. The heat generation inside each layer is considered to be as follows:

$$\dot{q}_j\left(\text{W/m}^3\right) = \begin{cases} \dot{q}_1 = 0.266 \times 10^6 \\ \dot{q}_2 = 0 \end{cases} \tag{14}$$

This is attributed to $200(\text{W/cm}^2)$ peak heat flux in the IGBTs. A 0.15 mm thick Arctic Silver 5 ($k = 8.7(\text{W/mK})$) is selected as the TIM layer between the dies, see Ref. [34]. The values of the interface contact conductance, convective heat transfer coefficient, and outer layer emissivity are then $\delta_1 = 11,600(\text{W/m}^2/\text{K})$, $h_{\text{c}} = 18,000(\text{W/m}^2/\text{K})$, and $\varepsilon = 0.8$, respectively.

Figure 5 shows the variations of the insulated surface temperature, T_{x_0}, and the considered surrounding fluid temperature, $T_{\text{sur.}}$, over time. The surrounding fluid temperature is considered to vary arbitrarily over time, as given by Eq. (13). The above-mentioned values for different parameters are taken into consideration to calculate the temperature field inside the media. As seen from Fig. 5, there is a good agreement between the analytical model and the obtained numerical data; the maximum and average relative difference are less than 6% and 4%, respectively. As such, the developed analytical model can predict the thermal characteristics of a composite medium under a general time-dependent boundary condition to comply with a given thermal transient duty cycle.

6 Conclusion

A new analytical model is presented for the solution of heat diffusion inside a multilayered composite medium. It is assumed that the outer boundary of the composite medium exchanges heat with a surrounding fluid via convection and radiation mechanisms. The temperature of the surrounding fluid is assumed to vary dynamically over time. As such, arbitrary time-dependent conjugate radiation–convection boundary condition is considered for the outer boundary of the studied medium. Arbitrary heat generation inside each layer and the thermal contact resistance between the layers are taken into consideration. Analytical outlines are presented for optimal design of multilayered systems, which undergo a thermal duty cycle. The present analytical results are verified successfully with the obtained independent numerical data.

Acknowledgment

This work was supported by Automotive Partnership Canada (APC), Grant No. APCPJ 401826-10. The authors would like to thank the support of the industry partner, Future Vehicle Technologies Inc. (British Columbia, Canada).

Nomenclature

$\mathbf{A}$ = matrix in Eq. (A4)
A_n = constant Eq. (A19)
A_{out} = constant in Eq. (7)
B_{out} = constant in Eq. (7)
Bi = combined Biot number = $Bi_r + Bi_c$
c_p = specific heat (J/kg/K)
C_{jn} = integration coefficient, Eq. (A3)
C_{out} = constant in Eq. (7)
D_{jn} = integration coefficient Eq. (A3)
E_n = constant Eq. (A14)
F = constant Eq. (A7)
Fo = Fourier number = $\alpha_1 t/x_1^2$
g_j = dimensionless heat generation inside the jth layer = $\mu_j \dot{q}(x)x_1^2/k_j(T_\infty - T_0)$
G_n = constant Eq. (A15)
H = constant Eq. (A10)
h_c = convective heat transfer coefficient (W/m^2/K)
h_r = radiative heat transfer coefficient (W/m^2/K)
i = complex variable = $\sqrt{-1}$
J_0 = zero-order Bessel function of the first kind
J_1 = first-order Bessel function of the first kind
k_j = thermal conductivity of the jth layer (W/m/k)K_j = dimensionless thermal conductivity ratio = $k_{j+1}/k_j M$ = number of layers
p = integer number ($p = 0$, 1, 2 for slabs, cylinders and spheres, respectively.)
$\mathbf{P}$ = matrix in Eq.(A5a) $\dot{q}_j$ = heat generation inside the jth layer (W/m^3)
$q^*_{\eta_j}$ = dimensionless interfacial heat flux at the interface of the jth layer$\eta = \eta_j$, = $\left(\partial\theta_j/\partial\eta\right)_{\eta_j = x_j/x_1}$ Eq. (A20)
R_{jn} = nth eigenfunction associated with $\lambda_n$for the jth layer Eq. (A2)
t = time (s)
T_a = amplitude of surrounding fluid temperature (K) Eq. (1)
T_j = temperature of the jth layer of the composite media (K)
T_0 = initial temperature of the system (K)
T_∞ = constant term of surrounding fluid temperature Eq. (1)
w = weight function Eq. (A8)
x = space coordinate (either rectangular, cylindrical or spherical)
x_j = values of space coordinate at the inner boundary surfaces $j = 0, 1, 2, ..., M$ (m)
x_M = space coordinate at the outer boundary surface
x_0 = coordinate origin
Y_0 = zero-order Bessel function of the second kind
Y_1 = first-order Bessel function of the second kind
ΔT_a = dimensionless amplitude of the imposed temperature $\Delta T_a = T_a/(T_\infty - T_0)$ Eq. (12)
ΔT_R = dimensionless number Eq. (6e)

Greek Symbols

α_j = thermal diffusivity of the jth layer (m^2/s)
Γ = function of Fo number Eq. (A12)
$\gamma(t)$ = arbitrary function of time Eq. (1)
δ_j = contact conductance between the jth and $j+1$th layers (W/m^2/K)
ε = outer surface emisivity
η = dimensionless coordinate = x/x_1
η_j = dimensionless coordinate at the boundaries = x_j/x_1
θ = dimensionless temperature = $(T - T_0)/(T_\infty - T_0)$
θ_j = dimensionless temperature of the jth layer= $\left(T_j - T_0\right)/(T_\infty - T_0)$
λ = separation constant
μ_j = dimensionless thermal diffusivity ratio
σ = Estephan–Boltzmann constant= 5.669×10^{-8}(W/m^2/K^4)
φ = phase shift, Eq. (A12)
ϕ_{jn} = solution to Eq. (A2) corresponding to λ_n
ψ_{jn} = solution to Eq. (A2) corresponding to λ_n
Ω = angular frequency (rad/s)
Ω = angular frequency of the surrounding fluid temperature (rad/s)
ω = dimensionless angular frequency
ω = dimensionless angular frequency of the surrounding fluid temperature $\omega = \Omega x_1^2/\alpha_1$ Λ_j = dimensionless conductance between the layers $\Lambda_j = \delta_j x_1/k_j$

Subscripts

c = convective
j = jth layer defined in the domain $x_{j-1} \le x \le x_j (j = 1, 2, ..., M)$
n = integer number positive
0 = initial condition
r = radiative

Abbreviations

Cond. = conduction
Conv. = convection
IGBT = integrated gate bipolar transistor
Max. = maximum
Rad. = radiation
Sur. = surrounding
TIM = thermal interface material

Appendix

Considering Eq. (7), any type of time-dependent surrounding temperature, $\gamma(t)$, can be decomposed into simple cosine functions using a cosine Fourier transformation [30]. As such, we develop the present model for a harmonic surrounding temperature, and the results can be generalized to cover the cases with arbitrary time variations in surrounding temperature by using a superposition. As such, the following expression is considered as the boundary condition on the outer surface of a composite medium.

$$A_{out} \times \frac{\partial\theta_M(\eta = x_M/x_1, Fo)}{\partial\eta} + B_{out} \times \theta_M(\eta = x_M/x_1, Fo) = C_{out} \times \cos(\omega Fo + \varphi) \quad \text{at} \quad \eta = \frac{x_M}{x_1}, Fo > 0, \quad B_{out} \neq 0 \tag{A1}$$

where A_{out}, B_{out}, and C_{out} are constant values; besides, φ is the phase shift. Therefore, when $\omega = 0$, Eq. (A1) addresses constant convective boundary conditions, which is the first term on the right-hand side of Eq. (7). When $\omega \neq 0$, Eq. (A1) can be used to find the solution of Eq. (7) for the cosine Fourier transformation of $\gamma(t)$by a superposition technique.

A.1. Solution to M-Layer Composite Medium. The system of eigenvalue problems associated with Eq. (6) is given below:

$$\mu_j \frac{1}{\eta^p}\frac{d}{d\eta}\left(\eta^p \frac{dR_{jn}}{d\eta}\right) = -\lambda_n^2 R_{jn} \quad j = 1, 2, 3, ..., M \tag{A2}$$

With the following homogeneous boundary conditions:

$$\frac{\partial R_1}{\partial\eta} = 0 \quad \text{at} \quad \eta = 0 \tag{A2a}$$

$$\frac{\partial R_j}{\partial\eta} = \Lambda_j\left[R_{j+1}\left(\eta = x_j/x_1\right) - R_j\left(\eta = x_j/x_1\right)\right] \quad j = 1, 2, 3, ..., (M-1) \tag{A2b}$$

$$\frac{\partial R_j\left(\eta = x_j/x_1\right)}{\partial\eta} = K_j \frac{\partial R_{j+1}\left(\eta = x_j/x_1\right)}{\partial\eta} \quad j = 1, 2, 3, ..., (M-1) \tag{A2c}$$

$$A_{\text{out}} \times \frac{\partial R_M(\eta = x_M/x_1)}{\partial \eta} + B_{\text{out}} \times R_M(\eta = x_M/x_1) = 0 \quad \text{at} \quad \eta = \frac{x_M}{x_1} \tag{A2d}$$

where R_{jn} is the eigenfunction in the jth layer associated with the nth eigenvalue, λ_n. The general solution of the above eigenvalue problem is in the form of

$$R_{jn}(\eta) = \begin{cases} R_{1n}(\eta) = \phi_{1n}(\eta) & 0 \le \eta \le 1 \\ R_{jn}(\eta) = C_{jn}\phi_{jn}(\eta) & +D_{jn}\psi_{jn}(\eta) \end{cases}$$
$$\frac{x_{j-1}}{x_1} \le \eta \le \frac{x_j}{x_1} \tag{A3}$$
$$j = 2, 3, ..., M$$

where the functions $\phi_{jn}(\eta)$ and $\psi_{jn}(\eta)$ are two linearly independent solutions of Eq. (A2). A list of the function $\phi_{jn}(\eta)$ and $\psi_{jn}(\eta)$ for slabs, cylinders and spheres can be found in Ref. [38].$\psi_{1n}(\eta)$ function is excluded from the solution, Eq. (A3), because of the boundary condition at the origin, see Eq. (6*b*). The remaining boundary conditions, Eq. A2(*a–d*) yields

$$\mathbf{Av} = \mathbf{0} \tag{A4}$$

where $\mathbf{v} = [1, C_{2n}, D_{2n}, C_{3n}, D_{3n}, ..., C_{Mn}, D_{Mn}]^T$, and the matrix $\mathbf{A}$ as well as its components are defined in Appendices A and B of our previous work [38]. However, $\mathbf{P_M}$ is defined as follows:

$$\mathbf{P}_M = \left[A_{\text{out}}\phi'_{Mn} + B_{\text{out}}\phi_{Mn} \quad A_{\text{out}}\psi'_{Mn} + B_{\text{out}}\psi_{Mn} \right]_{\text{at } \eta = \frac{x_M}{x_1}} \tag{A5a}$$

Equation (A4) yields $2M-1$ homogeneous simultaneous equations for $v_j, j = 1, 2, 3, \ldots, M$. Nontrivial solution exist if the determinant of the coefficients is zero,

$$\det \mathbf{A} = 0 \tag{A6}$$

Equation (A6) can be solved for the eigenvalues λ_n, see Ref. [38] for more detail. Rearranging Eq. (A2) the "discontinuous-weighting function" can be found by the method introduced by Yeh [19], see Ref. [38].

$$\frac{d}{d\eta}\left(F_j \eta^{\text{p}} \frac{dR_{jn}}{d\eta}\right) + \lambda_n^2 \eta^{\text{p}} \frac{F_j}{\mu_j} R_{jn} = 0$$
$$\frac{x_{j-1}}{x_1} \le \eta \le \frac{x_j}{x_1}, \quad j = 1, 2, 3, ..., M \tag{A7}$$

Note that F_j is a constant within the interval $x_{j-1}/x_1 \le \eta \le x_j/x_1$, yet unknown. Based on Refs. [19] and [22], the constants F_j should be determined such that the functions R_{jn} become orthogonal with respect to the discontinuous-weighting function $w(\eta)$. As such, the orthogonality factors are given below:

$$w(\eta) = \frac{\eta^{\text{p}}}{\mu_j} F_j \quad \frac{x_{j-1}}{x_1} \le \eta \le \frac{x_j}{x_1}, \quad j = 1, 2, ..., M \tag{A8}$$

Following Yeh [19], the following relationship is developed to evaluate the constants F_j, to form the weighting functions:

$$F_1 = 1, \quad F_j = \prod K_{j-1} \quad j = 2, 3, ..., M \tag{A9}$$

Now that the constants F_j are determined, the weighting function $w(\eta)$ is known. Therefore, any function $I(\eta)$ can be expanded inside the entire multilayered medium as follows:

$$I(\eta) = \sum_{n=1}^{\infty} H_n R_{jn}(\eta) \qquad 0 \le \eta \le \frac{x_M}{x_1} \tag{A10}$$

The expansion is carried out over the range of $0 \le \eta \le x_M/x_1$, spanning all M layers. The unknown coefficients H_n in Eq. (A10) are determined by a generalized Fourier analysis over the entire range of M layers and is given in the following form:

$$H_n = \frac{\sum_{j=1}^{M} \int_{\text{layer}j} I(\eta) w(\eta) R_{jn}(\eta) d\eta}{\sum_{j=1}^{M} \int_{\text{layer}j} w(\eta) \left[R_{jn}(\eta)\right]^2 d\eta} \tag{A11}$$

Using a separation-of-variables method, the temperature distribution inside the entire media is considered in the following form:

$$\theta_j(\eta, Fo) = \frac{C_{\text{out}}}{B_{\text{out}}} e^{i(\omega Fo + \varphi)} + \sum_{n=1}^{\infty} R_{jn}(\eta)\Gamma(Fo) e^{i(\omega Fo + \varphi)} \quad j = 1, 2, ..., M$$
$$B_{\text{out}} \neq 0 \tag{A12}$$

where $i = \sqrt{-1}$. Note that for convenience, the complex exponential function is assumed for the temperature distribution. Clearly, the final solution is the real part of the sought-after solution. Substituting Eq. (A12) into Eq. (6), and expanding the angular frequency over the entire medium, after some algebraic manipulation one obtains

$$\sum_{n=1}^{\infty} R_{jn}\left[\Gamma'(Fo) + \left(i\omega + \lambda_n^2\right)\Gamma(Fo) + iE_n - G_n \times e^{-i(\omega Fo + \varphi)}\right] = 0 \tag{A13}$$

where, based on Eq. (A11), the coefficients E_n and G_n can be determined by the following relationships:

$$E_n = \omega \frac{C_{\text{out}}}{B_{\text{out}}} \times \frac{\sum_{j=1}^{M} \int_{layerj} w(\eta) R_{jn}(\eta) d\eta}{\sum_{j=1}^{M} \int_{layerj} w(\eta) \left[R_{jn}(\eta)\right]^2 d\eta} \tag{A14}$$

$$G_n = \frac{\sum_{j=1}^{M} \int_{\text{layer}j} g_j(\eta) w(\eta) R_{jn}(\eta) d\eta}{\sum_{j=1}^{M} \int_{\text{layer}j} w(\eta) \left[R_{jn}(\eta)\right]^2 d\eta} \tag{A15}$$

Since in general R_{jn} is not zero, we must have

$$\Gamma'(Fo) + \left(i\omega + \lambda_n^2\right)\Gamma(Fo) + iE_n - G_n \times e^{-i(\omega Fo + \varphi)} = 0 \tag{A16}$$

The solution of Eq. (A16) is given by

$$\Gamma(Fo) = A_n e^{-\left(\lambda_n^2 + i\omega\right)Fo} - \frac{E_n\left(\omega + i\lambda_n^2\right)}{\lambda_n^4 + \omega^2} + \frac{G_n}{\lambda_n^2} \times e^{-i(\omega Fo + \varphi)} \tag{A17}$$

Substituting Eq. (A17) into Eq.(A12), and considering the real part of the solution

$$\theta_j(\eta, Fo) = \frac{C_{\text{out}}}{B_{\text{out}}} \times \cos(\omega Fo + \varphi) + \sum_{n=1}^{\infty} R_{jn}(\eta) \left\{ \begin{array}{l} A_n \times \cos(\varphi) \times e^{-\left(\lambda_n^2 Fo\right)} - \\ E_n \left\{ \dfrac{\omega \times [\cos(\omega Fo + \varphi)] - \lambda_n^2 \times [\sin(\omega Fo + \varphi)]}{\lambda_n^4 + \omega^2} \right\} + \dfrac{G_n}{\lambda_n^2} \end{array} \right\} \times j = 1, 2, \ldots, M \tag{A18}$$

The coefficients A_n can be obtained by using the initial condition, Eq.(6*a*), together with the orthogonality properties of the eigenfunctions

$$A_n = \frac{1}{\cos(\varphi)} \times \left\{ E_n \left[\frac{\omega \times \cos(\varphi) - \lambda_n^2 \times \sin(\varphi)}{\omega^2 + \lambda_n^4} - \frac{\cos(\varphi)}{\omega} \right] - \frac{G_n}{\lambda_n^2} \right\} \tag{A19}$$

The interfacial heat flux is determined by the following relationship:

$$q_j^* = \left. \frac{\partial \theta_j}{\partial \eta} \right|_{\eta_j = \frac{x_j}{x_1}} \tag{A20}$$

References

[1] O'Keefe, M., and Bennion, K., 2007, "A Comparison of Hybrid Electric Vehicle Power Electronics Cooling Options," IEEE Vehicle Power and Propulsion Conference, Arlington, TX, Sept. 9–12, pp. 116–123.

[2] Bennion, K., and Thornton, M., 2010, "Integrated Vehicle Thermal Management for Advanced Vehicle Propulsion Technologies," SAE Paper No. 2010-01-0836.

[3] Bennion, K., and Kelly, K., 2009, "Rapid Modeling of Power Electronics Thermal Management Technologies," Vehicle Power and Propulsion Conference, Dearborn, MI, Sept. 7–10, pp. 622–629.

[4] Bennion, K., and Thornton, M., 2010, "Integrated Vehicle Thermal Management for Advanced Vehicle Propulsion Technologies," SAE Paper No. NREL/CP-540-47416.

[5] Panão, M. R. O., Correia, A. M., and Moreira, A. L. N., 2012, "High-Power Electronics Thermal Management With Intermittent Multijet Sprays," Appl. Therm. Eng., **37**, pp. 293–301.

[6] Ghalambor, S., Agonafer, D., and Haji-Sheikh, A., 2013, "Analytical Thermal Solution to a Nonuniformly Powered Stack Package With Contact Resistance," ASME J. Heat Transfer, **135**(11), p. 111015.

[7] McGlen, R. J., Jachuck, R., and Lin, S., 2004, "Integrated Thermal Management Techniques for High Power Electronic Devices," Appl. Therm. Eng., **24**(8–9), pp. 1143–1156.

[8] Brooks, D., and Martonosi, M., 2001, "Dynamic Thermal Management for High-Performance Microprocessors," 7th International Symposium on High-Performance Computer Architucture (HPCA-7), Monterey, CA, Jan. 19–24, pp. 171–182.

[9] Yuan, T.-D., Hong, B. Z., Chen, H. H., and Wang, L.-K., 2001, "Thermal Management for High Performance Integrated Circuits With Non-Uniform Chip Power Considerations," 17th Annual IEEE Semiconductor Thermal Measurement and Management Symposium (Cat. No.01CH37189), San Jose, CA, pp. 95–101.

[10] Choobineh, L., and Jain, A., 2013, "Determination of Temperature Distribution in Three-Dimensional Integrated Circuits (3D ICs) With Unequally-Sized Die," Appl. Therm. Eng., **56**(1–2), pp. 176–184.

[11] Gurrum, S., and Suman, S., 2004, "Thermal Issues in Next-Generation Integrated Circuits," IEEE Trans. Device Mater. Reliab., **4**(4), pp. 709–714.

[12] Kelly, K., Abraham, T., and Bennion, K., 2007, "Assessment of Thermal Control Technologies for Cooling Electric Vehicle Power Electronics," 23rd International Electric Vehicle Symposium (EVS-23), Anaheim, CA, Dec. 2–5, Paper No. NREL/CP-540-42267.

[13] De Monte, F., 2000, "Transient Heat Conduction in One-Dimensional Composite Slab, A "Natural" Analytic Approach," Int. J. Heat Mass Transfer, **43**(19), pp. 3607–3619.

[14] Carslaw, H. S., and Jaeger, J. C., 1959, *Conduction of Heat in Solids*, Oxford University, London.

[15] Feng, Z. G., and Michaelides, E. E., 1997, "The Use of Modified Green's Functions in Unsteady Heat Transfer," Int. J. Heat Mass Transfer, **40**(12), pp. 2997–3002.

[16] Yener, Y., and Ozisik, M. N., 1974, "On the Solution of Unsteady Heat Conduction in Multi-Region Finite Media With Time-Dependent Heat Transfer Coefficient," 5th International Heat Transfer Conference, Tokyo.

[17] Mayer, E., 1952, "Heat Flow in Composite Slabs," ARS J., **22**(3), pp. 150–158.

[18] Tittle, C. W., 1965, "Boundary Value Problems in Composite Media: Quasi-Orthogonal Functions," Appl. Phys., **36**(4), pp. 1487–1488.

[19] Yeh, H. C., 1976, "Solving Boundary Value Problems in Composite Media by Seperation of Variables and Transient Temperature of a Reactor Vessel," Nucl. Eng. Des., **36**(2), pp. 139–157.

[20] Olek, S., Elias, E., Wacholder, E., and Kaizerman, S., 1991, "Unsteady Conjugated Heat Transfer in Laminar Pipe Flow," Int. J. Heat Mass Transfer, **34**(6), pp. 1443–1450.

[21] Olek, S., 1998, "Heat Transfer in Duct Flow of Non-Newtonian Fluid With Axial Conduction," Int. Commun. Heat Mass Transfer, **25**(7), pp. 929–938.

[22] Olek, S., 1999, "Multiregion Conjugate Heat Transfer," Hybrid Methods Eng., **1**, pp. 119–137.

[23] Fakoor-Pakdaman, M., Ahmadi, M., Bagheri, F., and Bahrami, M., 2014 "Dynamic Heat Transfer Inside Multilayered Packages with Arbitrary Heat Generations," Journal of Thermo. and Heat Trans., **28**(4), pp. 687–699.

[24] Antonopoulos, K. A., and Tzivanidis, C., 1996, "Analytical Solution of Boundary Value Problems of Heat Conduction in Composite Regions With Arbitrary Convection Boundary Conditions," Acta Mech., **118**(1–4), pp. 65–78.

[25] De Monte, F., 2004, "Transverse Eigenproblem of Steady-State Heat Conduction for Multi-Dimensional Two-Layered Slabs With Automatic Computation of Eigenvalues," Int. J. Heat Mass Transfer, **47**(2), pp. 191–201.

[26] Jain, P. K., and Singh, S., 2010, "An Exact Analytical Solution for Two-Dimensional, Unsteady, Multilayer Heat Conduction in Spherical Coordinates," Int. J. Heat Mass Transfer, **53**(9–10), pp. 2133–2142.

[27] Jain, P. K., and Singh, S., 2009, "Analytical Solution to Transient Asymmetric Heat Conduction in a Multilayer Annulus," ASME J. Heat Transfer, **131**(1), p. 011304.

[28] Miller, J. R., and Weaver, P. M., 2003, "Temperature Profiles in Composite Plates Subject to Time-Dependent Complex Boundary Conditions," Compos. Struct., **59**(2), pp. 267–278.

[29] Lu, X., Tervola, P., and Viljanen, M., 2006, "Transient Analytical Solution to Heat Conduction in Composite Circular Cylinder," Int. J. Heat Mass Transfer, **49**(1–2), pp. 341–348.

[30] Kreyszig, E., Kreyzig, H., and Norminton, E. J., 2012, *Advanced Engineering Mathematics*, Wiley, New York.

[31] Chapman, A. J., 1960, *Heat Transfer*, Macmillan, New York.

[32] Jakob, M., 1949, *Heat Transfer*, Wiley, New York.

[33] Zerkle, R. D., and Sunderland, J. E., 1965, "The Transint Temperature Distribution in a Slab Subject to Thermal Radiation," ASME J.Heat Transfer, **87**(1), pp. 117–132.

[34] Narumanchi, S., Mihalic, M., and Kelly, K., 2008, "Thermal Interface Materials for Power Electronics Applications," Itherm'08, Orlando, FL, May 28–31, Paper No. NREL/CP–540–42972.

[35] Iyengar, M., and Schmidt, R., 2006, "Analytical Modeling for Prediction of Hot Spot Chip Junction Temperature for Electronics Cooling Applications," ITHERM'06, San Diego, CA, May 30–Jun. 2, pp. 87–95.

[36] Mudawar, I., Bharathan, D., Kelly, K., and Narumanchi, S., 2009, "Two-Phase Spray Cooling of Hybrid Vehicle Electronics," IEEE Trans. Compon. Packag. Technol., **32**(2), pp. 501–512.

[37] Incropera, F. P., Dewitt, D. P., Bergman, T. L., and Lavine, A. S., 2007, *Introduction to Heat Transfer*, Wiley, New York.

[38] "WACKER® SILICONE HEAT SINK," http://www.tme.eu/en/Document/d92d7778128ac1dbd077dbba2b860f5b/P12-90%20TDS.pdf